JOURNAL OF MOLECULAR SPECTROSCOPY 170, 478–492 (1995)

The *a*-Type $K = 0$ Microwave Spectrum of the Methanol Dimer

F. J. LOVAS, S. P. BELOV,[1] M. YU. TRETYAKOV,[1]
W. STAHL,[2] AND R. D. SUENRAM

Molecular Physics Division, National Institute of Standards and Technology, Gaithersburg, Maryland 20899

The rotational spectrum of $(CH_3OH)_2$ has been observed in the region 4-22 GHz with pulsed-beam Fabry-Perot cavity Fourier-transform microwave spectrometers at NIST and at the University of Kiel. Each *a*-type $R(J)$, $K_a = 0$ transition is split into 15 states by tunneling motions for $(CH_3OH)_2$, $(^{13}CH_3OH)_2$, $(CH_3OD)_2$, $(CD_3OH)_2$, and $(CD_3OH)_2$. The preliminary analysis of the methyl internal rotation presented here was guided by the previously developed multidimensional tunneling theory which predicts 16 tunneling components for each $R(J)$ transition from 25 distinct tunneling motions. Several isotopically mixed dimers of methanol have also been measured, namely $^{13}CH_3OH$, CH_3OD, CD_3OH, and CD_3OD bound to $^{12}CH_3OH$. Since the hydrogen bond interchange motion (which converts a donor into an acceptor) would produce a new and less favorable conformation from an energy viewpoint, it does not occur and only 10 tunneling components are observed for these mixed dimers. The structure of the complex is similar to that of water dimer with a hydrogen bond distance of 2.035 Å and a tilt of the acceptor methanol of 84° from the O–H–O axis. The effective barrier to internal rotation for the donor methyl group of $(CH_3OH)_2$ is $V_3 = 183.0$ cm^{-1} and is one-half of the value for the methanol monomer (370 cm^{-1}), while the barrier to internal rotation of the acceptor methyl group is 120 cm^{-1}.

I. INTRODUCTION

Interest in the hydrogen bonding of the methanol dimer arises from the fact that it is among the simplest organic species which might exhibit hydrogen bonding, and by analogy to the water dimer, might also exhibit multidimensional tunneling splittings. By assuming that the methanol dimer would have the same geometry as the water dimer, with a nonbonded proton replaced by a methyl group, Ohashi and Hougen (*1*) developed tunneling splitting patterns and selection rules from group-theoretical considerations. They found that 25 distinct tunneling motions are feasible when the two monomers are identical, which produce 16 tunneling–rotational levels for each K_a subband. These include motions of the water dimer type, e.g., donor–acceptor interchange and lone-pair interchange in the bonding, as well as internal rotation of the inequivalent methyl groups.

Only a few dimers containing the methyl group have been studied previously, namely, CH_3OH–HCl (*2*), Ar–CH_3OH (*3*), CH_3OH–NH_2CHO (*4*), and CH_3OH–CO (*5*). In the case of the HCl and Ar complexes, the observed spectra were not consistent with just a single internal motion attributed to the methyl torsion. For CH_3OH–HCl the two states observed were interpreted as two vibrational states arising from lone-pair interchange in the hydrogen bond, while those for Ar–CH_3OH could

[1] Guest workers, 1992–1993. Permanent address: Institute of Applied Physics, Nizhny Novgorod, Russia.
[2] Institute for Physical Chemistry, University of Kiel, Kiel, Germany.

0022-2852/95 $6.00

not be modeled, perhaps due to the possibility of overall rotation of the methyl group in the complex as well as hindered rotation of the methyl group. The formamide and carbon monoxide complexes clearly show hindered internal rotation of the methyl group, but result in substantially reduced effective V_3 barrier heights when compared to the methanol monomer. Several of the present authors have suggested that a large amplitude motion of the OH group within the complex could provide an additional term in describing the internal rotation of the methyl group which might explain this apparent barrier reduction (*6*). Further interest in studying the methanol dimer thus arises in examining the effective barrier of the methyl group when it is located in either the donor or the acceptor unit.

II. EXPERIMENTAL DETAILS

Spectral measurements were carried out with a pulsed-beam Fabry-Perot cavity, Fourier-transform microwave spectrometer(*3*, *7*) of the Balle–Flygare type (*8*) in the frequency region 8–24 GHz. The initial spectra from methanol dimer were observed in the course of studying the CH_3OH–CO complex (*5*). A dual-inlet pulsed solenoid valve was used to deliver a supersonic molecular beam from a mixture of about 1 vol% of CO and CH_3OH, entrained in separate samples with Ar carrier gas, at a total pressure of 100 kPa (1 atm) to the center of a Fabry–Perot cavity. Molecular-beam pulses from a 0.5-mm nozzle orifice of 200- to 400-μs duration were employed with repetition rates up to 35 Hz. The molecular complex was polarized by a short microwave pulse when the microwave frequency was near resonant ($\Delta\nu < 400$ kHz) with a rotational transition of the complex. The dual inlet served to introduce the CO/Ar and CH_3OH/Ar samples to the nozzle in a continuous-flow manner, independently. This allowed chemical characterization of spectral transitions detected. In addition to the CH_3OH–CO species, other known dimeric species observed were CO–H_2O (*9*) and Ar–CH_3OH (*3*), and subsequently methanol dimer. It was relatively easy to distinguish between each of these by alternately cutting off the flow of each of the inlets or by using Ne as carrier gas. In order to confirm the assignment for the K_a rotational quantum number, Stark fields were applied to the molecular beam by two parallel plates (26 × 26 cm) with a separation of about 26 cm by using voltages up to +5 and −5 kV on each plate.

While the initial measurements of methanol dimer were accomplished with the old configuration described above, most of the final measurements and those of the isotopically substituted forms were made with a new nozzle configuration and a change in the microwave components as described in a recent report on the CH_3NO_2–H_2O complex (*10*). The major changes involved use of a nozzle behind one of the mirrors, which allows the molecular beam to travel colinearly with the cavity axis. Also, implementation of the pulse sequence circuit from the Kiel group (*11*) has been incorporated to allow phase-coherent digitization of the first IF signal (30 MHz) at a clock frequency of 8 MHz. The free-induction-decay signal from the cavity was digitized in 0.125-μs increments for 4096 channels. Typically, 2–200 pulses were signal averaged, after subtracting a background microwave pulse from each signal pulse, in order to yield reasonable signal-to-noise ratios. The averaged data were then Fourier transformed to obtain the amplitude spectrum with a resolution element of 2 kHz and linewidth of 2–5 kHz. The measurement precision and accuracy is estimated to be 0.5 kHz. This new configuration provides a signal-to-noise ratio of better than 100 for a single pulse on the strongest lines of methanol dimer.

The configuration used in Kiel is described in Ref. (*12*) and is similar to the final configuration employed at NIST.

To produce the various isotopically substituted CH_3OH dimers, we used commercially available samples of normal CH_3OH, CH_3OD, CD_3OH, CD_3OD, and $^{13}CH_3OH$. Both Ne and Ar carrier gases were used; neon provided the strongest signals and argon provided the narrowest linewidths.

III. OBSERVED SPECTRUM AND ASSIGNMENT

The initial searches provided several groups of *a*-type *R*-branch transitions which exhibited second-order Stark effect qualitatively characteristic of K_a = 0, 1, and 2 transitions. Figure 1 shows an automated scan of 100 MHz with a resolution of 0.4 MHz for the J = 2–1 region taken at NIST. At NIST the $R(J)$ transitions of methanol dimer from J = 2–1 to 5–4 were measured. Due to the detected presence of higher K_a transitions and some uncertainty in the qualitative Stark effect measurements, we felt that it was important to obtain J = 1–0 transitions which would exhibit only the K_a = 0 level. Since this region of the spectrum was not conveniently accessible at NIST, the group at Kiel joined our efforts by measuring the J = 1–0 transitions. These measurements provided a clear assignment for the higher J measurements from NIST for K_a = 0. For both the $(CH_3OH)_2$ and the $(^{13}CH_3OH)_2$ species only 15 K_a = 0 transitions were found for each rotational state, while theory predicted 16 transitions (*1*): four *A*, four *G*, and eight *E* symmetry species from the permutation-inversion group G_{36}. In addition, the J = 2–1 measurements of the CH_3OD–CH_3OH, $(CH_3OD)_2$, $(^{13}CH_3OH)_2$ and mixed ^{13}C–^{12}C species were made in Kiel, and subsequent work was performed at NIST. Figure 2 shows an automated scan from Kiel of the J = 2–1 transitions for $(CH_3OH)_2$, CH_3OD–CH_3OH, and $(CH_3OD)_2$ on a common frequency scale to illustrate the changes in splitting as well as the center of the patterns.

Table I lists the measurements for CH_3OH dimer, Table II for the $^{13}CH_3OH$ dimer, and Tables III and IV for the mixed $^{13}CH_3OH$–$^{12}CH_3OH$ and $^{12}CH_3OH$–$^{13}CH_3OH$

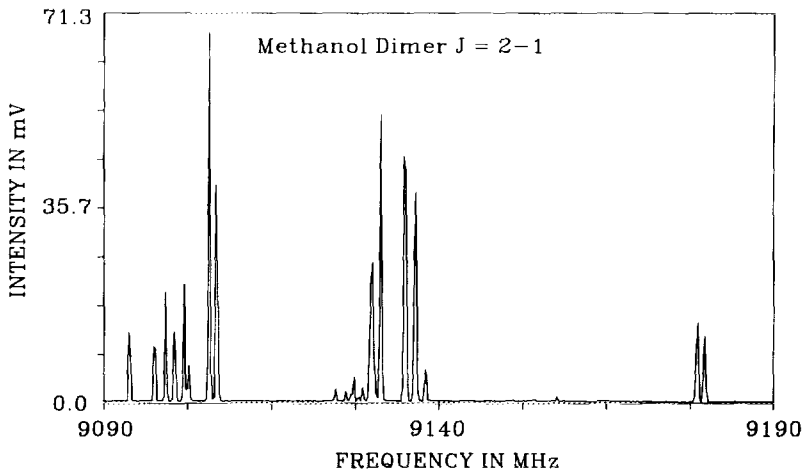

FIG. 1. Low-resolution 100-MHz scan of the J = 2–1 region of methanol dimer with the spectrometer at NIST. Ten molecular beam pulses were averaged for each frequency step of 0.4 MHz. Only the largest intensity point of the transformed signal is plotted for each step, so that two or more closely spaced lines are not resolved.

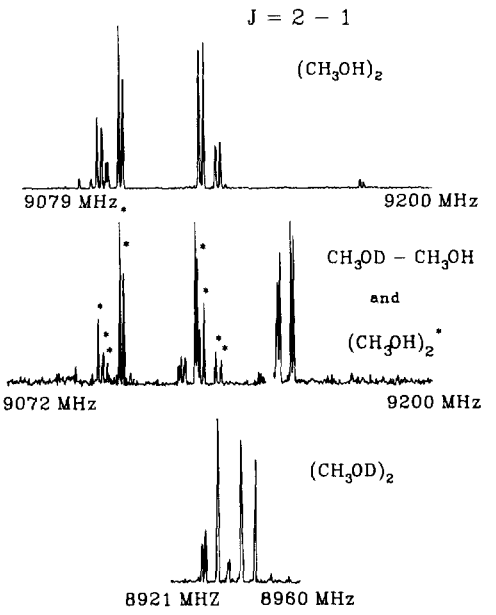

FIG. 2. Low-resolution broadband scans of the $J = 2$–1 regions for methanol dimer, CH_3OD–CH_3OH, and $(CH_3OD)_2$ taken with the Kiel spectrometer.

species. The first thing to note in Table I is a constant difference between adjacent transitions for the E states and A states listed in the last column. The same results are obtained for $(^{13}CH_3OH)_2$ in Table II, and the differences are nearly identical to those in Table I. If one compares Tables III and IV to Tables I and II it is clear that this J-independent splitting pattern vanishes, so that it is unique to identical dimer units. This constant difference, regardless of the J state, thus arises from a motion which vanishes for the $^{12}C/^{13}C$ mixed dimers, and in fact we believe that this splitting is due to the interconversion motion which exchanges the donor–acceptor roles of each methanol monomer. The J independence of these splittings is also consistent with the "bottom–top" and "top–bottom" selection rules for such a motion which inverts the sense of the μ_a dipole moment component. The fact that these splittings range from 0 to 190 kHz between various pairs of components for the A and E state transitions, shown in the last column of Tables I and II, suggests that there are several paths which contribute to the interchange.

In order to identify the symmetry species of the observed transitions, careful intensity measurements were performed of the $J = 2$–1 transition in Kiel and of the $J = 3$–2 and 5–4 transitions at NIST. These are listed in Table V. The G_{36} character table is given in Table I of Ref. (*13*), and the statistical weights are shown in parentheses for the symmetry species A_1 (36), A_2 (28), A_3 (36), A_4 (28); E_1 (16), E_2 (16), E_3 (20), E_4 (12); and G (64). Comparison of the statistical weights with the observed intensities allowed us to identify the E, G, and A groups. Since one of the E lines is about twice as strong as the others, we conclude that two E states are degenerate to within the observed linewidth (about 4 kHz). We can thus explain the missing 16th state. The symmetry state labeling in Tables I, II, and V follows the labeling sequence described in the following paper by Ohashi and Hougen (*14*) with the numerical sublabels of

TABLE I

Observed Transitions of $(CH_3OH)_2$ and Average First Differences

Sym.[a]	J = 1 - 0 MHz	J = 2 - 1 MHz	J = 3 -2 MHz	J = 4 - 3 MHz	J = 5 - 4 MHz	Diff.[b] kHz
E 1,2	4549.8348	9099.248	13647.774	18194.967	22740.328	\
						32.6
E 2,1	4549.8678	9099.280	13647.808	18194.992	22740.367	/
E 1,2*	4550.5203	9100.609	13649.833	18197.741	22743.860	0
E 4,4	4551.2377	9101.986	13651.677	18199.762	22745.691	\
						86.0
E 3,3	4551.3215	9102.072	13651.761	18199.854	22745.775	/
E 4,4	4551.5401	9102.602	13652.606	18201.016	22747.282	\
						90.5
E 3,3	4551.6316	9102.691	13652.697	18201.106	22747.373	/
G a	4553.1299	9105.768	13657.416	18207.572	22755.719	\
						564 J
G b	4553.6845	9106.883	13659.104	18209.845	22758.603	/
G c	4565.2766	9129.902	13693.230	18254.606	22813.383	\
						688 J
G d	4565.9526	9131.260	13695.286	18257.383	22816.902	/
A 2,4	4567.6762	9134.802	13700.643	18264.546	22825.867	\
						191.3
A 3,1	4567.8667	9134.995	13700.834	18264.736	22826.059	/
A 4,2	4568.4570	9136.348	13702.970	18267.680	22829.839	\
						144.4
A 1,3	4568.6010	9136.493	13703.115	18267.824	22829.983	/

[a] The numerical labels, 1 - 4 refer to the lower state and upper state, respectively. These alternate in sequence for the even and odd lower J states for all of the A state lines and the E1 and E2 states. The a, b, c, d values only serve to distinguish the G states. The transition labeled with an asterisk is blended and the E1 and E2 assignments are uncertain.

[b] Average difference between adjacent states. Measured uncertainties are 2 kHz (2σ).

the E and A species alternating with J since these transitions are across the interconversion tunneling splitting (bottom-to-top or top-to-bottom energy level). The intensity measurements in Table V show that the neighboring $A1/A2$ and $A3/A4$ levels and the $E3/E4$ levels alternate in relative intensity between adjacent J'–J'' transitions as predicted by the group-theoretical arguments in Ref. (*14*).

Since the transition frequencies and relative intensities were insufficient to identify the dominant tunneling motions and paths considered in Ref. (*1*), we carried out further isotopic measurements with pure CH_3OD, CD_3OH, and CD_3OD in order to observe their dimeric forms and mixed with CH_3OH to obtain spectra of the monosubstituted forms of each. The measured transitions of the $(CH_3OD)_2$ and $CH_3OD_{(d)}$–$CH_3OH_{(a)}$ species are shown in Table VI, where the subscripts "d" and "a" refer to the donor and acceptor units, respectively. Spectra for $CH_3OH_{(d)}$–$CD_3OH_{(a)}$ are listed in Table VII, those for $CD_3OH_{(d)}$–$CH_3OH_{(a)}$ are given in Table VIII, and the CD_3OH dimer spectum is shown in Table IX. Table X lists the observed transitions of the $(CD_3OD)_2$ species. Examination of the reduction in the splitting patterns, particularly for the monosubstituted CD_3OH species, led us to conclude that the largest splittings were due to internal rotation of each methyl group, and when combined with a structural analysis (described in a later section), the acceptor unit was shown to produce the larger splitting. Thus, the isotopic studies were a key in isolating the source of the major splittings.

IV. ROTATION-INTERNAL ROTATION ANALYSIS

In the present paper we will present a simplified treatment of the $K = 0$ spectrum of methanol dimer which considers only the splittings due to two inequivalent, but

TABLE II

Observed Transitions for $(^{13}CH_3OH)_2$ and Average First Differences

Sym.[a]	J = 1 - 0 MHz	J = 2 -1 MHz	Diff.1[b] kHz
E 1,2	4364.6300	8728.8367	\
			31.5
E 2,1	4364.6608	8728.8689	/
E 1,2*	4365.3091	8730.1874	0.0
E 4,4	4365.8487	8731.2274	\
			82.6
E 3,3	4365.9315	8731.3097	/
E 4,4	4366.1919	8731.9200	\
			89.7
E 3,3	4366.2813	8732.0099	/
G a	4367.6040	8734.7254	\
			565.4 J
G b	4368.1682	8735.8587	/
G c	4378.6326	8756.6484	\
			694.6 J
G d	4379.3259	8758.0400	/
A 2,4	4380.8156	8761.1090	\
			183.8
A 3,1	4380.9996	8761.2926	/
A 4,2	4381.6003	8762.6648	\
			142.9
A 1,3	4381.7430	8762.8078	/

[a] The numerical labels, 1 - 4 refer to the lower state and upper state, respectively. These alternate in sequence for the even and odd lower J states for all of the A state lines and the E1 and E2 states. The a, b, c, d values only serve to distinguish the G states. The transition labeled with an asterisk is blended and the E1 and E2 assignments are uncertain.

[b] Average difference between adjacent states. Measured uncertainties are 2 kHz (2σ).

noninteracting, methyl rotors which are analyzed independently with a one-top Hamiltonian program. A more general treatment of the tunneling motions based on an extension of the water dimer treatment is given in the following paper by Ohashi and Hougen (*14*). Each of the J'–J'' $K = 0$ patterns was reduced to a two-top problem as shown in Table XI by using the $J = 1$–0 data from the second column of Table I. The first average shown in column 3 of Table XI involves only the adjacent lines with a constant splitting as a function of J for the A and E states. The fourth column of Table XI gives the average of all adjacent pairs in the E, G, and A states. The column labeled "Ave. 3" in the fifth column of Table XI shows an essentially equal splitting caused by one methyl top, added to the initial splitting (last column of Table XI or "Ave. 4") caused by the second methyl group. This last column was derived by taking one-third of the A (EA and AA labels) and E (EE and AE labels) splitting in the Ave. 3 column and adding it to the E (EE or EA labels) frequency. It should be noted that the second step in the averaging of adjacent lines of a given species label (column 4 of Table XI) shows the five components which are characteristic of molecules with two inequivalent tops where a subset of the E levels are split by an interaction term between the two tops (see schematic energy diagram in Ref. (*14*)). The third average

TABLE III

Observed Transitions of $CH_3OH_{(d)}$–$^{13}CH_3OH_{(a)}$

Sym.[a]	J = 1-0 MHz	J = 2-1 MHz	J = 3-2 MHz	J = 4-3 MHz
E 3	4459.7381	8919.0382	13377.458	17834.545
E 3	4460.3774	8920.3269	13379.410	17837.185
E 4	4461.0679	8921.6164	13381.122	17839.057
E 4	4461.3689	8922.2231	13382.040	17840.298
E 2 (G)	4462.8504	8925.2138	13386.606	17846.530
E 2 (G)	4463.3849	8926.2903	13388.234	17848.730
E 1 (G)	4474.4647	8948.2863	13420.824	17891.437
E 1 (G)	4475.1136	8949.5901	13422.796	17894.095
A 2, 1	4476.8465	8953.0563	13427.992	17901.023
A 1, 2	4477.5737	8954.5177	13430.204	17904.005

[a] Symmetry labels from the group G_{18}, and states correlating to G levels of G_{36} labeled (G).

in column 5 of Table XI is characteristic of the two-equivalent-tops problem or where no top–top interaction occurs. After reducing the data for each rotational transition as shown in Table XI, we analyzed the A and E components in the last column with the largest splitting as a one-top problem and similarly the lower frequency and higher frequency pair of lines shown in column 5 of Table XI, i.e., the lines labeled EE and AE and the higher frequency pair labeled EA and AA. The Hamiltonian employed was

$$H = A''P_a^2 + B''P_b^2 + CP_c^2 + D_{ab}[P_aP_b + P_bP_a] - \Delta_J\mathbf{P}^4 + FP_\alpha^2 - (1 - \cos 3\alpha)[\tfrac{1}{2}V_3 + F_v\mathbf{P}^2]. \quad (1)$$

TABLE IV

Observed Transitions for $^{13}CH_3OH_{(d)}$–$CH_3OH_{(a)}$

Sym.	J = 1-0	J = 2-1	J = 3-2	J = 4-3
E 3	4453.6982	8906.9534	13359.319	17810.343
E 3	4454.3901	8908.3467	13361.428	17813.190
E 4	4455.0349	8909.5480	13363.009	17814.912
E 4	4455.3885	8910.2566	13364.080	17816.331
E 2 (G)	4456.8157	8913.1394	13368.479	17822.333
E 2 (G)	4457.3997	8914.3125	13370.250	17824.747
E 1 (G)	4468.3568	8936.0851	13402.560	17867.155
E 1 (G)	4469.0774	8937.5351	13404.750	17870.106
A 2,1	4470.7411	8940.8568	13409.721	17876.726
A 1,2	4471.5361	8942.4552	13412.141	17879.981

[a] Symmetry labels from the group G_{18}, and states correlating to G levels of G_{36} labeled (G).

TABLE V

Intensity Measurements for $K_a = 0$ Transitions of CH_3OH Dimer

Symmetry Species[a]	J= 2 - 1 Rel. Int.[b]	J= 3 - 2 Rel. Int.[b]	J = 5 - 4 Rel. Int.[b]
E 2,1	6.1	6.5	7.5
E 1,2	6.6	8.6	7.8
E 2,1*	11.8	14.5	13.5
E 4,4	9.6	4.8	5.0
E 3,3	5.5	9.3	8.5
E 4,4	7.7	6.0	5.0
E 3,3	5.6	9.5	8.0
G a	15.9	36.9	25.
G b	15.0	35.8	30.
G c	16.65	41.3	18.
G d	14.7	41.8	19.
A 4,2	8.6	24.2	10.
A 1,3	7.3	30.8	12.
A 2,4	8.0	21.1	9.
A 3,1	7.0	24.4	12.

[a] The numerical sub-state labels change with the lower state J value. The first value corresponds to the lower state and the second value applies to the upper state. The sequence shown is correct for the J = 2-1 transition, and the ordering for the J = 3-2 and 5-4 should be reversed for the A levels and E1 and E2 levels.

[b] Relative intensities in arbitrary units apply only for a given J' - J" transition.

In the above equation the parameters from Lin and Swalen (*15*) are defined as

$$A'' = A + B - B', \qquad B'' = (1 - r)I_\alpha AB/\rho^2(505\ 379.05), \qquad C'' = C \quad (2)$$

$$D_{ab} = \rho_a\rho_b(B - A)/\rho^2, \qquad \rho_a = \lambda_a I_\alpha/I_a, \qquad \rho_b = \lambda_b I_\alpha/I_b,$$

$$\text{and} \qquad \rho = [\sum_x (\lambda_x I_\alpha/I_x)^2]^{1/2} \quad (3)$$

$$F = h/8\pi^2 r I_\alpha, \qquad r = 1 - \sum_x (\lambda_x^2 I_\alpha/I_x). \quad (4)$$

See Refs. (*15*, *16*) for further description of this Hamiltonian. The molecular constants employed in the fits should be considered "effective" and they include the dependence of both the barrier, V_3, and the dimensionless parameter, ρ, on the rotational quantum numbers J and K. Since only the $K = 0$ transitions have been assigned, it was necessary to fix a number of the coefficients in Eq. (1). The A value was fixed at the best structural value, and we assumed methyl top moments of inertia, I_α, of 3.2 u Å^2 for CH_3 and 6.4 u Å^2 for CD_3. A fixed value of the angle between each methyl group and

TABLE VI

Rotational Transitions of $CH_3OD_{(d)}$–$CH_3OH_{(a)}$ and $(CH_3OD)_2$

	$CH_3OD_{(d)}$–CH_3OH (a)		$(CH_3OD)_2$	
Sym.	J= 2 - 1	J = 3 -2	J = 2 - 1	J = 3 - 2
E	9123.4839	13684.1744	8930.1970	13394.010
E	9124.2017	13685.2625	8930.4523	13394.408
E	9125.4108	13686.9068	8931.3499	13395.683
E	9125.7661	13687.4461	8931.5013	13395.879
G	9128.7083	13691.9185	8934.8904	13401.032
G	9129.3032	13692.8190	8935.1356	13401.399
G	9153.3563	13728.5387	8942.0339	13411.570
G	9154.1143	13729.6852	8942.3029	13411.980
A	9157.5287	13734.8067	8946.1238	13417.730
A	9158.3592	13736.0631	8946.4348	13418.201

the a-axis of the complex, $\theta_d = 52°$ and $\theta_a = 65°$ for the donor and acceptor, respectively, were derived from the structure fit and determine the direction cosines, e.g., $\lambda_a = \cos\theta_a$ and $\lambda_b = \cos(90 - \theta_a)$. From these equations we then derived A'', D_{ab}, F, and ρ from the equations of Lin and Swalen (*15*) and used them, and C as well, as fixed values in the analysis.

Initially, we fit the rotation–internal rotation averaged lines with a typical high-barrier Hamiltonian and fixed values of I_α and θ; however, the reduced barrier term, $s = 4V_3/9F < 20$, indicated that this was inappropriate, except for the CD_3 species

TABLE VII

Rotational Transitions of $CH_3OH_{(d)}$–$CD_3OH_{(a)}$

Sym.	J= 3 - 2	J = 4 -3
E	12655.429	16871.247
E	12656.095	16872.146
E	12656.334	16872.352
E	12656.739	16872.902
G	12662.185	16880.230
G	12662.890	16881.199
G	12667.750	16887.458
G	12668.526	16888.509
A	12674.043	16895.872
A	12675.005	16897.179

TABLE VIII

Rotational Transitions of $CD_3OH_{(d)}$–$CH_3OH_{(a)}$

Sym.	J= 2 - 1	J= 3 - 2	J = 4 -3
E	8338.490	12506.566	16673.229
E	8338.797	12506.997	16673.761
E	8339.313	12507.812	16674.899
E	8339.351	12507.841	16674.913
G	8339.544	12508.133	16675.294
G	8340.146	12509.023	16676.527
G	8363.297	12543.492	16721.940
A	8363.933	12544.534	16723.330
G	8364.491	12545.337	16724.382
A	8365.200	12546.360	16725.794

TABLE IX

Rotational Transitions for $(CD_3OH)_2$

Sym.[a]	J = 3 - 2 MHz	J = 4 - 3 MHz
E 1,2	11601.570[b]	15466.341[b]
E 2,1	11601.643	15466.429
E 1,2*	11601.688	15466.476
E 4,4	11602.094	15467.052
E 3,3	11602.111	15467.069
E 4,4	11602.147	15467.118
E 3,3	11602.195	15467.167
G a	11602.448	15467.503
G b	11602.975	15468.220
G c	11611.060	15478.870
G d	11611.814	15479.889
A 2,4	11611.855	15479.946
A 3,1	11611.922	15480.016
A 4,2	11612.621	15480.980
A 1,3	11612.677	15481.040

[a] The numerical labels, 1 - 4 refer to the lower state and upper state, respectively. These alternate in sequence for the even and odd lower J states for all of the A state lines and the E1 and E2 states. The a, b, c, d values only serve to distinguish the G states. The transition labeled with an asterisk is blended and the E1 and E2 assignments are uncertain.

[b] triplet.

TABLE X

Rotational Transitions for $(CD_3OD)_2$

Sym.	J= 3 - 2	J = 4 - 3 MHz
E	11395.734	15192.050
E	11395.813	15192.153
G	11396.410	15192.950
G	11396.460	15193.026
G	11399.445	15196.940
G	11399.525	15197.061
A	11400.105	15197.828
A	11400.192	15197.950

which have a larger s value. These fits yielded standard deviations of 0.5 to 2 MHz, which was much larger than the measurement accuracy of 2 kHz, and most of the isotopic species treated had reduced barrier values of $s = 10$–15. Following these fits, we employed the program described by Kleiner *et al.* (*16*), which appears to function well at much lower barrier heights, by assuming values of A'', C, F, and ρ derived from Eqs. (2)–(4) and assuming a symmetric top model with $B = C = (B + C)/2$.

TABLE XI

CH_3OH Dimer $J = 1$–0 Splitting Reduction to Two Inequivalent Methyl Tops

Sym.[a]	J= 1 - 0	Ave. 1	Ave. 2	Ave. 3 (top 1)	Ave. 4 (top 2)
E 1,2	4549.8348	4549.8513	4550.1858 $E_{\mp}E_{\pm}$	4550.8093 EE	4551.6753 E
E 2,1	4549.8678				
E 1,2*	4550.5203	4550.5203			
E 4,4	4551.2377	4551.2796	4551.4328 $E_{\pm}E_{\pm}$	2.5979	
E 3,3	4551.3215				
E 4,3	4551.5401	4551.5859			
E 3,3	4551.6316				
G a	4553.1299	4553.1299	4553.4072 AE	4553.4072 AE	14.7845
G b	4553.6845	4553.6845			
G c	4565.2766	4565.2766	4565.6146 EA	4565.6146 EA	4566.4598 A
G d	4565.9526	4565.9526			
A 2,4	4567.6762	4567.7715	4568.1503 AA	2.5357	
A 3,1	4567.8667			4568.1503 AA	
A 4,2	4568.4570	4568.5290			
A 1,3	4568.6010				

[a] See footnote a for Table I.

TABLE XII

Rotational and Internal Rotation Analysis for the CH_3OH, $^{13}CH_3OH$, and CD_3OH Species[a]

Species	(B+C)/2[b] [MHz]	B" [MHz]	D_{ab}[c] [MHz]	D_J [kHz]	V_3 donor [cm^{-1}]	V_3 acceptor [cm^{-1}]	F_v [MHz]	σ [kHz]
$(CH_3OH)_2$	2278.375	3484.682	-3831.33	23.67	-	120.4(1)	-40.45	6
	2275.883	2728.072	-2417.85	20.25	183.6 l[d]		-20.4	3
	2283.282	2694.340	-2423.90	24.48	207.1 u[d]		63.4	1
$(^{13}CH_3OH)$	2185.439	3329.193	-3707.30	21.69	-	120.4	-40.45[c]	6
	2183.195	2600.503	-2301.34	19.58	183.2 l		-20.4[c]	1
	2189.925	2602.115	-2323.09	26.02	190.8 u		0.	1
$^{13}CH_3OH_{(d)}$-$CH_3OH_{(a)}$	2230.117	3400.006	-3769.41	23.02	-	120.3	-40.45[c]	11
	2227.768	2667.270	-2375.00	20.30	182.7 l		-23.84	1
	2234.818	2640.739	-2380.81	24.71	203.3 u		44.70	1
$CH_3OH_{(d)}$-$^{13}CH_3OH_{(a)}$	2233.157	3410.053	-3767.78	23.11	-	120.2	-42.7	1
	2230.773	2668.173	-2375.30	19.95	185.2 l		-15.43	2
	2237.851	2630.239	-2381.12	23.09	211.2 u		76.96	1
$CH_3OH_{(d)}$-$CD_3OH_{(a)}$	2110.821	3272.671	-3490.11	20.76	-	96.1	-76.0	2
	2110.188	2534.407	-2216.07	24.0	192.1 l		0.	1
	2112.177	2537.140	-2217.68	25.5	192.2 u		0.	1
$CD_3OH_{(d)}$-$CH_3OH_{(a)}$	2087.075	3200.558	-3481.69	22.33	-	122.9	-26.5	7
	2084.975	2495.746	-2202.95	19.65	173.7 l		0.	3
	2091.224	2504.102	-2207.97	24.04	182.1 u		0.	13
$(CD_3OH)_2$	1934.617	2967.793	-3186.47	21.98	-	104.2	0.	17
	1934.081	2325.775	-2025.50	21.67	182.9 l		0.	1
	1935.690	2330.486	-2032.88	22.6	183.0 u		0.	1

[a] Moments assumed: I_α (CH_3) = 3.2 uÅ^2 and I_α (CD_3) = 6.4 uÅ. θ_d = 52° θ_a = 65°
[b] Since only K = 0 data were fit, we assumed B = C.
[c] Fixed value.
[d] l = lower frequency group, and u = upper frequency group

Since we have been unable to completely assign the $K = 1$ spectra, we fit the spectra as a symmetric top with B'', D_J, V_3, and in some cases F_v, which is a distortion term for the barrier height. The results for all of the isotopic species are summarized in Table XII for the OH species and Table XIII for the OD species. Note that the effective barrier, V_3, for the donor shows a variation of about 10% between various isotopic species while the acceptor shows changes up to 65%, and the magnitudes are a factor of two to four smaller than V_3 of methanol monomer. There are several other things to note about the V_3 barriers in Tables XII and XIII, i.e., when CD_3 is substituted for

TABLE XIII

Rotational and Internal Rotation Analysis for the CH_3OD and CD_3OD Species[a]

Species	(B+C)/2[b] [MHz]	B" [MHz]	D_{ab}[c] [MHz]	D_J [kHz]	V_3 donor [cm^{-1}]	V_3 acceptor [cm^{-1}]	σ [kHz]
$CH_3OD_{(d)}$-$CH_3OH_{(a)}$	2284.132	3468.681	-3832.62	22.63	-	125.9	44
	2281.687	2725.943	-2420.38	18.90	199.4 l[d]		2
$(CH_3OD)_2$	2234.186	3380.151	-3639.84	23.25	-	161.1	26
	2233.239	2660.164	-2292.01	21.85	197.8 l		4
$(CD_3OD)_2$	1899.904	2935.854	-3089.70	20.41	-	131.9	8
	1899.696	2294.260	-1972.29	20.19	189.8 l		1

[a] Moments assumed: I_α (CH_3) = 3.2 uÅ^2 and I_α (CD_3) = 6.4 uÅ. θ_d = 52° θ_a = 65°
[b] Since only K = 0 data were fit, we assumed B = C.
[c] Fixed value.
[d] l = lower frequency group. The upper frequency group had nearly identical splitting and V_3 barrier.

the acceptor CH_3, the acceptor barrier is reduced, and when OD is substituted for the acceptor OH, the effective acceptor barrier increases. For this latter case, OD substition, Fig. 2 shows the dramatic reduction in splittings between $CH_3OD_{(d)}$–CH_3OH (middle trace) and $CH_3OD_{(d)}$–$CH_3OD_{(a)}$ (bottom trace). This change in splittings is evidence for large amplitude motion effecting the A and E splitting through a kinetic effect rather than through the potential, as discussed by Fraser *et al.* (*6*).

Earlier we described the use of relative intensity measurements for assigning the E, G, and A subsets of tunneling states, as well as finding alternating intensities in the E and A subsets as a function of rotational transition. In most of the isotopically substituted species, the E, G, and A tunneling state labels were consistent with the calculated spin weights associated with these symmetry species. However, in the case of $CD_3OH_{(d)}$–$CH_3OH_{(a)}$, whose spectrum is given in Table VIII, there were several anomalies. First, the relative intensities of the four highest frequencies, the last four lines of Table VIII, indicated that the assignment of the tunneling states should be A, G, A, G rather than the as shown G, A, G, A. We employed the labels as shown based on the internal rotation analysis, since the assignment according to intensities fit poorly; Ohashi and Hougen (*14*) also agree with this assignment. We have not found an explanation for this anomaly.

VI. STRUCTURE

Since only the $K = 0$ spectrum of methanol dimer has been assigned, we can provide only a rather limited structure analysis, which requires a number of assumptions.

By employing the usual assumption that the monomer geometries are unchanged in complex formation and assuming that the donor proton bonds symmetrically to the HOC angle of the acceptor, only three structural parameters are required. These are $R_{H\text{-}O}$, and the two angles θ, a rotation defined by the H–O and bisector of the second methanol HOC angle, and ϕ, the dihedral angle, as defined in Fig. 3. Fits were carried out using the $I_b + I_c$ moments of inertia of only the species containing the OH group, resulting in one standard deviation values of 0.24 u Å^2. The parameters determined in the fit are $R_{H\text{-}O}$ = 2.034(9) Å, θ = 95.3(6)°, and ϕ = ±54.6(2)°, and the derived O–O distance is 2.98(2) Å. Figure 2 clearly shows that the CH_3OD–CH_3OH species is anomalous since its pattern of transitions is higher than the corresponding $(CH_3OH)_2$ transitions, suggesting a shorter O–D bonding distance. In

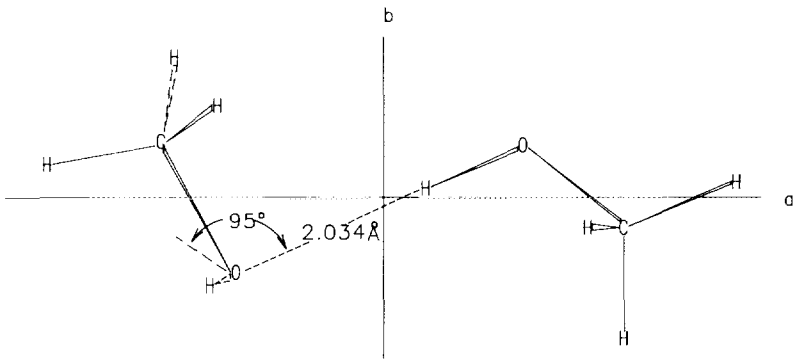

FIG. 3. Structure for methanol dimer.

contrast, the $(CH_3OD)_2$ and $(CD_3OD)_2$ moments of inertia are larger than the structural predictions, which suggests some angular changes as well.

VII. DISCUSSION

We report here the microwave spectrum of 10 isotopic forms of the methanol dimer which exhibits multidimensional tunneling splittings with rather large internal rotation splitting from methyl torsion of the inequivalent tops. The moments of inertia derived from the rotational constants were employed in the structural analysis, and a geometry of modest accuracy has been determined. In order to fit the observed "tunneling reduced" rotational spectra to near measurement accuracy, an extended IAM treatment was necessary, but due to oversimplification of the model, this analysis must be considered to provide "effective" molecular parameters such as the V_3 potential barrier. The value of $V_3 = 183$ cm^{-1} reported here for the donor methyl group is about a factor of two smaller than that for methanol (373 cm^{-1}), and V_3 for the acceptor methyl group is 120 cm^{-1}, which is a surprisingly large change to attribute to changes in electron density in the methanol subunit considering the weakness of the bonding interaction. Other methanol complexes which have been studied, wherein the internal rotation has also been treated, are methanol–formamide (*4*), with a value $V_3 = 231.0$ cm^{-1}, and methanol–carbon monoxide (*5*), with $V_3 = 183$ cm^{-1}. Fraser *et al.* (*6*) have shown that librational motion of the OH can substantially effect the A–E splittings, and we cannot determine independently the contribution to the potential term, V_3, versus the kinetic term, F, which depends on the reduced moment of inertia.

As a means of estimating the relative strength of weak hydrogen (or van der Waals) bonds, the pseudo-diatomic model (*17*) is often invoked in calculating the stretching force constant, $k_s = 16\pi^2 R_{cm}^2 \mu_D^2 B_D^4 / D_J$. For CH_3OH dimer, $R_{cm} = 3.477$ Å and $D_J = 23.67$ kHz, and we determined that $k_s = 1.83$ N m^{-1}, which may be compared to a value of 10.8 N m^{-1} for water dimer (*18*), suggesting that methanol dimer has a substantially weaker hydrogen bond. On the other hand, a literature search revealed several *ab initio* structure and potential studies of methanol dimers and polymers (*19–21*) which indicate that both the binding energy and the oxygen–oxygen distance should be nearly the same in water dimer and methanol dimer. For example, at the CEP-31G** level, Anwander *et al.* (*20*) calculate an O–O distance of 3.01 Å and an interaction enengy of 19.3 kJ/mol (4.6 kcal/mol) for water dimer, while the corresponding values for methanol dimer are 3.02 Å and 17.3 kJ/mol (4.1 kcal/mol). Experimentally, the O–O distance for water dimer is 2.972 Å, compared to the theoretical value of 2.979 Å. However, the theoretical results for the angular orientation of methanol dimer differ quite significantly, with values ranging from $\theta = 132°$ (*19*) to 175° (*20*) compared with our derived value of 95°.

One additional complex containing methanol is currently under study in our laboratory, namely, CH_3OH–HCN. It has an effective V_3 barrier near 100 cm^{-1} (*22*) with the methanol in the acceptor site. Thus, large internal rotation effects seem to be fairly common in dimeric complexes of methanol. Understanding the origin of these effects could have important implications in condensed phase chemistry and biological systems since reaction rates may be substantially modified by cooperative effects of the hydrogen bonding in systems containing methyl rotors.

ACKNOWLEDGMENTS

The authors are grateful to J. T. Hougen and N. Ohashi for many helpful comments on the analysis and manuscript.

RECEIVED: October 19, 1994

REFERENCES

1. N. OHASHI AND J. T. HOUGEN, *J. Mol. Spectrosc.* **163,** 86–107 (1994).
2. P. COPE, A. C. LEGON, AND D. J. MILLEN, *Chem. Phys. Lett.* **112,** 59–64 (1984).
3. R. D. SUENRAM, F. J. LOVAS, G. T. FRASER, J. Z. GILLIES, C. W. GILLIES, AND M. ONDA, *J. Mol. Spectrosc.* **137,** 127–137 (1989).
4. F. J. LOVAS, R. D. SUENRAM, G. T. FRASER, C. W. GILLIES, AND J. ZOZOM, *J. Chem. Phys.* **88,** 722–729 (1988).
5. F. J. LOVAS, S. P. BELOV, M. YU. TRETYAKOV, J. ORTIGOSO, AND R. D. SUENRAM, *J. Mol. Spectrosc.* **167,** 191–204 (1994).
6. G. T. FRASER, F. J. LOVAS, AND R. D. SUENRAM, *J. Mol. Spectrosc.* **167,** 231–235 (1994).
7. F. J. LOVAS AND R. D. SUENRAM, *J. Chem. Phys.* **87,** 2010–2020 (1987).
8. T. J. BALLE AND W. H. FLYGARE, *Rev. Sci. Instrum.* **52,** 33–45 (1981).
9. D. YARON, K. I. PETERSON, D. ZOLANDZ, W. KLEMPERER, F. J. LOVAS, AND R. D. SUENRAM, *J. Chem. Phys.* **92,** 7095–7109 (1990).
10. F. J. LOVAS, N. ZOBOV, G. T. FRASER, AND R. D. SUENRAM, *J. Mol. Spectrosc.*, in press (1995).
11. U. ANDRESEN, private communication; J.-U. GRABOW, Ph.D. thesis, Universität Kiel, 1992.
12. U. ANDRESEN, H. DREIZLER, J.-U. GRABOW, AND W. STAHL, *Rev. Sci. Instrum.* **61,** 3694–3699 (1990).
13. D. D. NELSON, JR., AND W. KLEMPERER, *J. Chem. Phys.* **87,** 139–149 (1987).
14. N. OHASHI AND J. T. HOUGEN, *J. Mol. Spectrosc.* **170,** 493–505 (1995).
15. C. C. LIN AND J. S. SWALEN, *Rev. Mod. Phys.* **31,** 841–892 (1959).
16. I. KLEINER, M. GODEFROID, M. HERMAN, AND A. R. W. MCKELLAR, *J. Mol. Spectrosc.* **142,** 238–253 (1990); I. KLEINER, J. T. HOUGEN, R. D. SUENRAM, F. J. LOVAS, AND M. GODEFROID, *J. Mol. Spectrosc.* **148,** 38–49 (1991); I. KLEINER, J. T. HOUGEN, R. D. SUENRAM, F. J. LOVAS, AND M. GODEFROID, *J. Mol. Spectrosc.* **153,** 578–586 (1992).
17. D. J. MILLEN, *Can. J. Phys.* **63,** 1477–1479 (1985).
18. T. R. DYKE, K. M. MACK, AND J. S. MUENTER, *J. Chem. Phys.* **66,** 498–510 (1977).
19. J. E. DEL BENE, *J. Chem. Phys.* **55,** 4633–4636 (1971).
20. E. H. S. ANWANDER, M. M. PROBST, AND B. M. RODE, *Chem. Phys.* **166,** 341–360.
21. Y.-C. TSE, M. D. NEWTON, AND L. C. ALLEN, *Chem. Phys. Lett.* **75,** 350–356 (1980).
22. F. J. LOVAS AND J. SOBHANADRI, private communication.